A Weighted Osteon Morphotype Score Outperforms Regional Osteon Percent Prevalence Calculations for Interpreting Cortical Bone Adaptation

John G. Skedros,[1,2]* Casey J. Kiser,[1,2] and Shaun D. Mendenhall[1,2]

[1]*Bone and Joint Research Laboratory, Department of Veterans Affairs Medical Center, Salt Lake City, UT*
[2]*Department of Orthopaedic Surgery, The University of Utah, Salt Lake City, UT*

KEY WORDS bone adaptation; load history; strain mode; osteon; collagen fiber orientation

ABSTRACT Using circularly polarized light microscopy, we described a weighted-scoring method for quantifying regional distributions of six secondary osteon morphotypes (Skedros et al.: Bone 44 (2009) 392–403). This osteon morphotype score (MTS) strongly correlated with "tension" and "compression" cortices produced by habitual bending. In the present study, we hypothesized that the osteon MTS is superior to a relatively simpler method based on the percent prevalence (PP) of these osteon morphotypes. This was tested in proximal femoral diaphyses of adult chimpanzees and habitually bent bones: calcanei from sheep, deer, and horses, radii from sheep and horses, and third metacarpals (MC3s) from horses. Sheep tibiae were examined because their comparatively greater torsion/shear would not require regional variations in osteon morphotypes. Predominant collagen fiber orientation (CFO), a predictor of regionally prevalent/predominant strain mode, was quantified as image gray levels (birefringence). Ten PP calculations were conducted. Although PP calculations were similar to the osteon MTS in corroborating CFO differences between "tension" and "compression" cortices of the chimpanzee femora and most of the habitually bent bones, PP calculations failed to show a compression/tension difference in equine MC3s and sheep radii. With the exception of the prevalence of the "distributed" osteon morphotype, correlations of PP calculations with CFO were weak and/or negative. By contrast, the osteon MTS consistently showed positive correlations with predominant CFO. Compared with the osteon MTS and predominant CFO, regional variations in PP of osteon morphotypes are not stronger predictors of nonuniform strain distributions produced by bending. Am J Phys Anthropol 144:41–50, 2011.

The microstructure of limb bone shafts has been extensively scrutinized over the past few decades, with a major goal in physical anthropology of finding histological correlates of local load history (e.g., osteon density) that can be applied to the fossil record or to bones that are not amenable to in vivo strain measurement. For example, studies in physical anthropology that are aimed at identifying regional histological adaptation in diaphyses of limb bones often rely on correlation analyses between specific microstructural/ultrastructural characteristics and strain-related characteristics of load history at a local level (e.g., between different bones of the same skeleton or between anterior and posterior cortices of the same transverse section at mid-diaphysis) (Abbott et al., 1996; Kalmey and Lovejoy, 2002; Skedros et al., 2004, 2006; Drapeau and Streeter, 2006; Pfeiffer et al., 2006; Ural and Vashishth, 2006; McFarlin et al., 2008). An important advance in studies of osteonal bone adaptation is the identification of regional variations in the population densities of specific types of secondary osteons (Haversian systems) that can significantly influence local mechanical properties (Hiller et al., 2003; Bigley et al., 2006). In a recent study using circularly polarized light (CPL) images of plane-parallel transverse sections of limb bone diaphyses, we evaluated two weighted-score methods for detecting mechanically important regional variations in six secondary osteon morphologic variants (morphotypes) that are based on birefringent patterns (Skedros et al., 2009). As described by Martin et al. (1996), these birefringent patterns are attributed to variations in lamellar collagen organization/orientation, ranging from "hoop" osteons with a peripheral ring of highly oblique-to-transverse collagen to "distributed" osteons with highly oblique-to-transverse collagen patterns distributed across the osteon wall (see Fig. 1).

The results of our recent study showed that a modification of Martin et al.'s (1996) scoring scheme (see Fig. 1) strongly correlated with the nonuniform strain-mode distribution (tension, compression, and shear) in bones that receive habitual bending (sheep, deer, and equine calcanei; sheep and equine radii). Additionally, we found that the modified osteon morphotype score (MTS) strongly correlated with regional variations in predominant collagen fiber orientation (CFO), which can

Additional Supporting Information may be found in the online version of this article.

Grant sponsors: Doctor's Education Research Fund of Orthopaedic Hospital, University of Southern California Department of Orthopaedic Surgery, Los Angeles, California, USA.

*Correspondence to: John G. Skedros, Utah Bone and Joint Center, 5323 South Woodrow Street, Suite 202, Salt Lake City, UT 84107. E-mail: jskedros@utahboneandjoint.com

Received 22 December 2009; accepted 24 May 2010

DOI 10.1002/ajpa.21365
Published online 18 August 2010 in Wiley Online Library (wileyonlinelibrary.com).

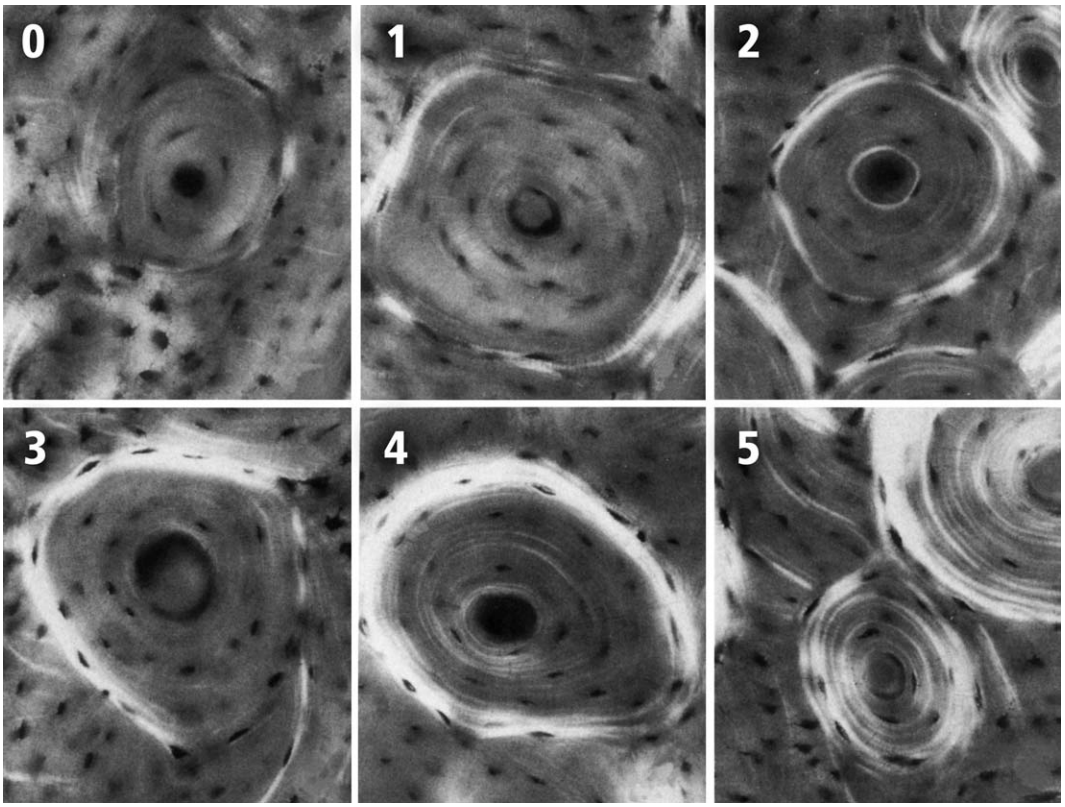

Fig. 1. Osteon morphotype scoring scheme used in this study with examples of each birefringence pattern ("morphotype"). These six categories are further defined in the text: **0** = category **N**, a dark osteon with no birefringent lamellae; **1** = category **OWI**, a combination of OI and OW; **2** = category **OW**, similar to O but the birefringent ring is weak; **3** = category **OI**, similar to O but the birefringent ring is incomplete; **4** = category **O** osteon with dark interior and strongly birefringent peripheral lamellae; **5** = category **D**, birefringent lamellae are distributed throughout the wall of the osteon. These images are reproduced from the original study of Martin et al. (1996). The section from which the images were obtained was 100 μm thick, and each photomicrograph in this montage is to the same scale (field width 200 μm) and illustrates one of the six birefringence categories used in this study. (Reproduced with permission from Martin et al., Bone, 1996, 19, 165–171, ©Elsevier Science, Inc.).

reliably reflect adaptation for a regionally prevalent strain mode (e.g., "tension" vs. "compression" cortices) of habitual bending.

Abbreviations

A	anterior (=cranial and dorsal)
Ca	caudal
CFO	collagen fiber orientation
CPL	circularly polarized light
Cr	cranial
D	distributed osteon morphotype or dorsal
L	lateral
M	medial
MC3	third metacarpal
MTS	morphotype score
N	dark (no hoop) osteon morphotype
N.On/T.Ar	secondary osteon population density (no./mm^2)
O	complete/strong hoop osteon morphotype
OI	incomplete/strong hoop osteon morphotype
On.B.Ar/T.Ar	fractional area of secondary osteonal bone
OW	weak/incomplete hoop osteon morphotype
OWI	weak incomplete hoop osteon morphotype
P	palmar, plantar, or posterior (=caudal)
PMMA	polymethyl methacrylate
PP	percent prevalence
T	total osteons
T.Ar	total area of image excluding porous spaces
WMGL	weighted mean gray level (refers to CFO, see above)

To establish the reliability of this modified osteon MTS (referred to below as "the osteon MTS") as a means for interpreting load history, it is important to investigate its limitations. In this study, we sought to determine if the osteon MTS is superior for detecting regional adaptation to habitual bending when compared with a relatively simpler method of quantification based on the regional percent prevalence (PP) of one or more of the six osteon morphotypes. We further hypothesized that the osteon MTS would correlate more strongly with predominant CFO than the PP of one or more of the six osteon morphotypes. These hypotheses were tested by analyzing the same osteons from our previous study of CPL images from the "tension," "compression," and "neutral axis" regions of the diaphyses of the following habitually bent bones: calcanei from sheep, deer, and horses, and radii from sheep and horses (Skedros et al., 2009). In this study, we also evaluated femora of chimpanzee to place this method in an anthropological context. As in our previous study, sheep tibiae and equine MC3s were also examined because they experience comparatively greater load complexity that, presumably because of increased prevalence of torsion/shear (resulting from broadly shifting neutral axes), would not require the same regional mechanical enhancements provided by different osteon morphotypes. Regional birefringence variations between the CPL images are

expressed as differences in mean gray levels, which represent differences in predominant CFO. Because predominant CFO, expressed as mean image gray levels, can reliably reflect adaptation for a regionally prevalent strain mode, this value was used to define the presence of regional strain-mode-related matrix adaptation (Boyde and Riggs, 1990; Skedros and Hunt, 2004; Skedros et al., 2004, 2007b, 2009).

MATERIALS AND METHODS

Bones, bone regions, strain data, and sectioning

Seven bones of each type listed below were obtained from left limbs of skeletally mature deer, sheep, and horses, and one femur was obtained from each of eight skeletally mature chimpanzees. The equine bones were from Quarter horses (4–8 years old) that were set to pasture. These animals had no history of racing or race training. Male Rocky Mountain mule deer (*Odocoileus hemionus hemionus*; estimated age range: 3–4 years) were from their natural habitat. The male sheep (*Ovis aries*) (2 years old, breed is crossed Suffolk/Hampshire and Rambouillet) were domesticated and were from large pastures. None of the animals had evidence of skeletal disease.

The chimpanzee sample included four females (8–39 years old, mean: 28.0 ± 14.4), three males (18–31 years old, mean: 25.3 ± 6.7) (entire sample: 26.7 ± 11.0), and one adult animal of unknown age and sex. The chimpanzees were born in the colony from the Yerkes National Primate Research Center, Lawrenceville, Georgia. The chimpanzee bones were from animals that had been kept in large cages with features of natural habitat. None of the chimpanzees had diseases or conditions that affect the musculoskeletal system. External morphologic parameters and trabecular architecture of all femora were quantified in previous studies (Kuo et al., 1998, 2003; Skedros and Baucom, 2007). None of the bones had evidence of significant arthritis, and there were no angular deformities.

For purposes of the comparisons made in this study, the bones can be separated into two groups: (1) those that experienced "habitual" bending ("tension/compression" bones) and (2) those that experienced significant torsion superimposed on bending and/or axial compression. The habitually bent bones include: (A) sheep calcanei (Lanyon, 1974; Skedros et al., 1997), (B) equine calcanei (Skedros et al., 1997), (C) Rocky Mountain mule deer calcanei (Su et al., 1999), (D) sheep radii (Lanyon and Baggott, 1976; Lanyon et al., 1979), (E) equine radii (Biewener et al., 1983; Riggs et al., 1993a), and (F) chimpanzee proximal femoral diaphyses (Skedros and Baucom, 2007). In these bones, axial (i.e., along the long axis of the bone) compression and axial tension are prevalent/predominant in opposing dorsal/plantar cortices (calcanei), caudal/cranial cortices (radii), or medial/lateral cortices (chimpanzee femora). These load categories conceptualize and simplify the characteristic loading patterns of the analyzed regions. As explained below and in our previous study (Skedros et al., 2009), regional variations in the populations of osteon morphotypes would be expected in habitually bent bones but not in bones that receive relatively more prevalent/predominant torsion.

It was more difficult to specifically place the chimpanzee femora in the habitual bending group. This is because neither in vivo nor ex vivo strain data are available for the adult chimpanzee proximal femur. There are, however, indirect data suggesting the presence of a habitual bending moment across the chimpanzee femoral neck (Kalmey and Lovejoy, 2002) that loads the proximal femoral diaphysis in medial-lateral bending (Skedros and Baucom, 2007). Consequently, habitual loading of the chimpanzee proximal femoral diaphysis is likely somewhere between the relatively simple bending group and the more complex torsion/shear group. In this perspective, the direction of habitual bending in the chimpanzee proximal femoral diaphysis was considered a priori to be in the medial-lateral direction, with prevalent/predominant tension in the lateral cortex and prevalent/predominant compression in the medial cortex; the neutral axis is somewhere in between these regions (see Fig. 2).

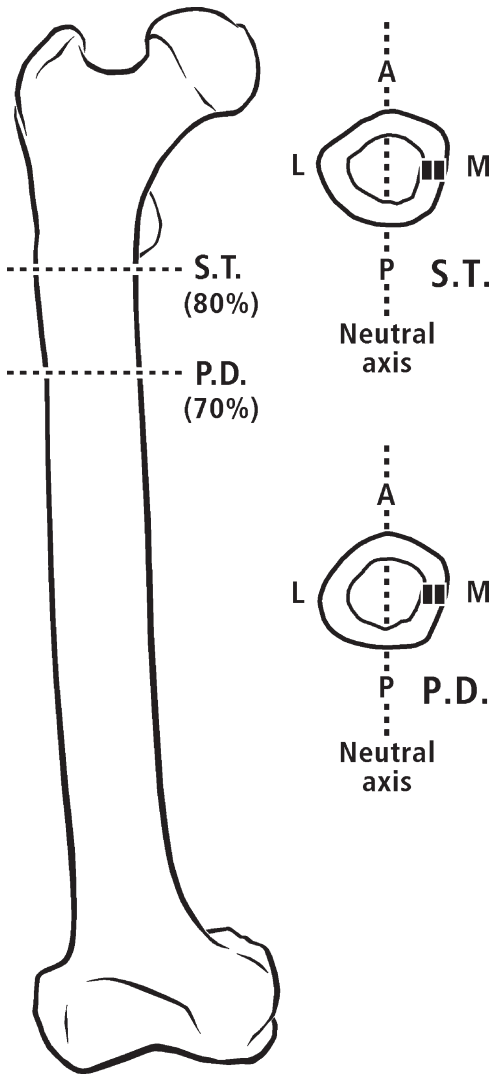

Fig. 2. Drawing of a right chimpanzee femur showing the two section locations, drawings of the representative sections, and the four cortical locations. The small rectangles shown in the lateral cortices serve as an example of where the microscopic images were obtained in each cortex. The dashed line drawn in the anterior-posterior direction shows the general location of the estimated neutral axis (NA) in the two sections. With respect to the NA, habitual compression is medial and habitual tension is lateral. A, anterior; L, lateral; P, posterior; M, medial; ST, subtrochanteric (80% diaphysis); PD, proximal diaphysis (70% diaphysis).

Compared with the "tension/compression" bones (calcanei, radii, and chimpanzee proximal femoral diaphyses), the equine MC3s and sheep tibiae receive relatively more torsion during their habitual loading. Consequently, although these bones also receive bending, shear strains from torque are relatively prevalent (Lanyon and Bourn, 1979; Gross et al., 1992; Lieberman et al., 2004).

A 5-mm-thick segment was cut transversely from each nonprimate bone, and two from each chimpanzee femur (see Fig. 2). Using percentages of shaft length as described previously (Skedros et al., 1994a, 1997), horse and deer calcanei were each cut at the proximal third (toward the joint) of the diaphysis. Equine and sheep radii, sheep tibiae, and equine MC3s were each cut at 50% of their overall length. From each of the chimpanzee femora, two 1.0–1.5 cm transversely cut segments were obtained: (1) one just distal to the inferior base of lesser trochanter (80%) and (2) one from 70% proximal diaphysis (Kuo et al., 1998). All segments of the bones were embedded in polymethyl methacrylate (PMMA), without decalcification or staining, using standard methods (Emmanual et al., 1987).

Using a low-speed diamond blade saw (Exact, West Germany) and continuous water irrigation, a 1.0-mm-thick transverse section was obtained from each PMMA-embedded segment. One surface of each of these sections was milled to a high luster finish (Reichert/Jung Ultramiller). The milled surface was then mounted with cyanoacrylate glue onto a glass slide, and the opposite side was milled to achieve a uniform overall thickness of 100 ± 5 μm (Skedros et al., 1996).

Circular polarized light analysis

Milled sections were analyzed for CFO using CPL according to the method of Boyde and Riggs (1990), where they were viewed in the light microscope after being placed between appropriately crossed left- and right-hand polarizing filters (HNCP37 $\times$ 0.030-inch (0.762 mm) filter; Polaroid Corporation, Norwood, MA) (Neville, 1980). Regional differences in CFO were quantified in terms of corresponding differences in the transmitted light intensity, where darker gray levels represent relatively more longitudinal CFO and brighter gray levels represent relatively more oblique-to-transverse CFO (Boyde and Riggs, 1990; Bromage et al., 2003).

Gray level values and other microstructural parameters were quantified in the anterior, posterior, medial, and lateral locations of each section. "Anterior" and "posterior," respectively, are used as surrogates for the actual, but various, terms used for the opposing sagittal-plane cortices in the calcanei (dorsal and plantar), radii (cranial and caudal), and equine MC3 (dorsal and palmar). Two to four 50$\times$ images (512 by 480 pixels; $\sim$ 2.3 mm by 2.3 mm images) were analyzed in each cortical location. A 4$\times$ objective was used with a 0.10 numerical aperture (Olympus "D-Plan 4$\times$, 0.10, 160/0.17"), which provided a 15.5 μm depth of field. For each image, care was taken to avoid circumferential lamellar bone. Grayscale images from each cortex were captured and stored onto a rewritable compact disc.

Regional differences in CFO were inferred from corresponding differences in the intensity of transmitted light (based on the relative intensity of birefringence), which are expressed as weighted mean gray levels (WMGLs). The methods used to determine a WMGL from each image have been described elsewhere (Skedros et al., 1996; Bloebaum et al., 1997). In this study, regional variations in image gray levels are referred to as differences in "CFO/WMGL."

Microstructure analysis: Osteon selection criteria and osteon morphotype score

The population density of the secondary osteons (N.On/T.Ar, no./mm^2) and area fraction of the secondary osteons (On.B.Ar/T.Ar, expressed as a percentage) were quantified from the digitized images. The On.B.Ar/T.Ar values include the areas of the central canals (Haversian canals) of the osteons. Methods for selecting secondary osteons are described in our previous study (Skedros et al., 2009). Each secondary osteon that was both complete and met these criteria was placed into one of six categories, based on birefringence pattern (see Fig. 1).

Each osteon morphotype was then assigned a numerical value, where five of the six numerical values are based on the presence and strength of the peripheral highly birefringent (i.e., "bright") pattern, or "hoop." The osteons also have designated abbreviations (in parentheses and bold print) that are coupled with numerical values as follows: **dark (N)** = 0 (no "hoop"), **weak incomplete hoop (OWI)** = 1, **weak complete hoop (OW)** = 2, **incomplete strong hoop (OI)** = 3, **strong complete hoop (O)** = 4, and **distributed (D)** = 5 (birefringent lamellae are distributed throughout the wall of the osteon). The "distributed" morphotypes included the "alternating" and "bright" osteons described by Bromage et al. (2003) and Ascenzi and Bonucci (1968). The numerical values for the osteon morphotypes were tabulated, and the "osteon MTS" was calculated for each image. This was accomplished by determining the number of each specific osteon type, multiplying each type by its respective assigned value (0, 1, 2, ...5), summing the products, and then dividing by the total number of quantified osteons (Martin et al., 1996).

The PP of one or more of the osteon types was also determined for each image. This was accomplished by dividing the selected osteon morphotype(s) by the total quantified osteons in the images taken in each cortical location (i.e., anterior, posterior, etc.). This method did not include any weighted scoring. The 10 PP calculations that were evaluated are shown in Supporting Information Figure S1 and in each of the Tables.

Statistical analysis

In each species, all possible pairwise comparisons between the cortical regions for each parameter (CFO/WMGL, N.On/T.Ar, On.B.Ar/T.Ar, osteon MTS, and PP calculations) were assessed for statistical significance using a Kruskal-Wallis multiple-comparison ANOVA design (Sokal and Rohlf, 1995; Hintze, 2004). An alpha level of $\leq$0.0083 was considered statistically significant, which represents a Bonferroni correction for the multiple comparisons. Correlation coefficients (r values) were determined for comparisons of CFO/WMGL with osteon MTSs or PP calculations. In all cases, these included the four cortical regions in each bone. The magnitudes of the resulting correlation coefficients (r) were interpreted according to the classification of Hinkle et al. (1979): ranges of 0.9–0.99, 0.7–0.89, 0.5–0.69, 0.3–0.49, and 0.0–0.29 are interpreted as representing very high, high, moderate, low, and little if any correlation, respectively.

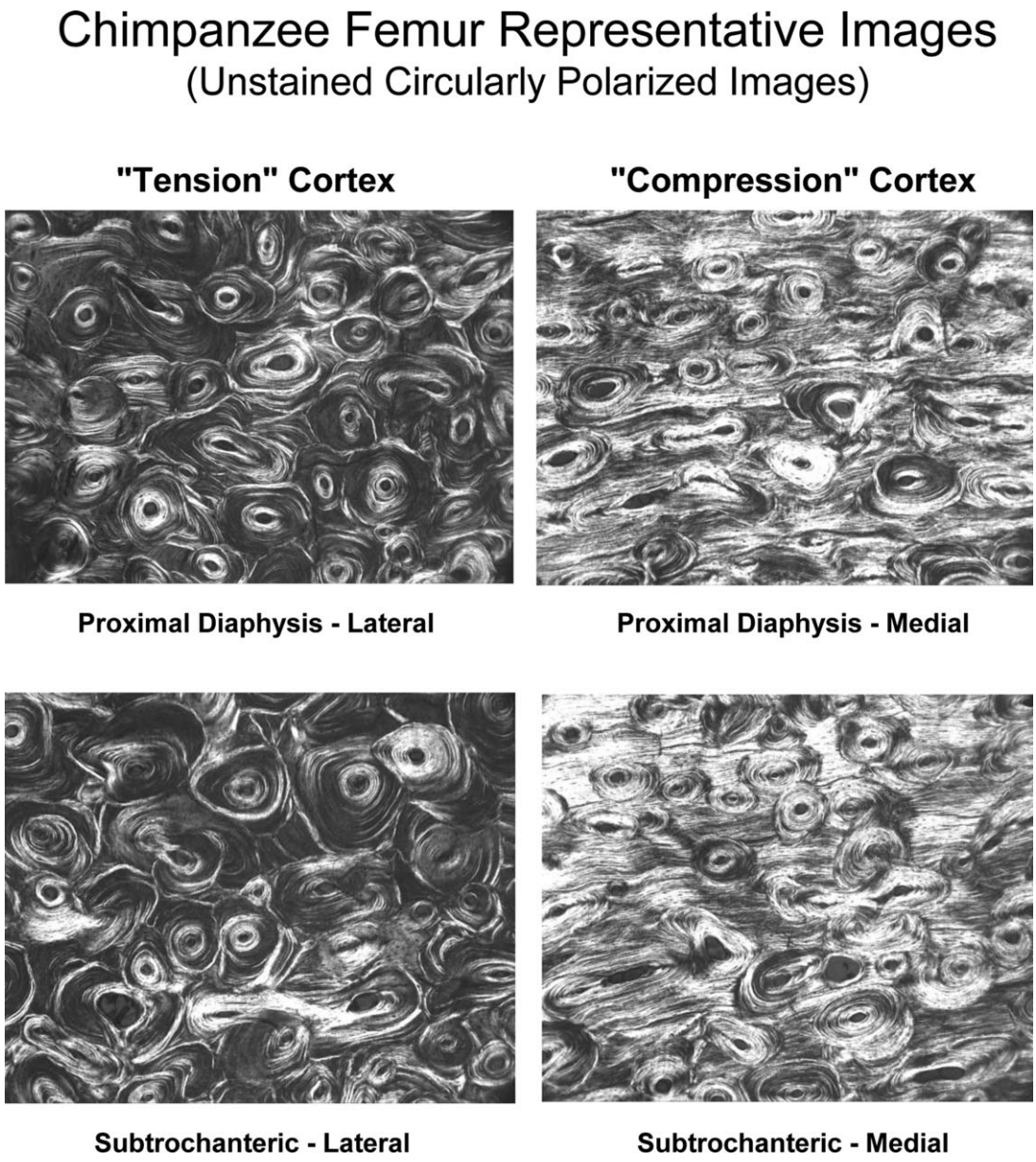

Fig. 3. Representative circularly polarized light images taken from the proximal diaphyseal cross sections of an adult chimpanzee femur. At left is an image from the lateral "tension" cortex that shows generally darker osteons, which are quantified as lower osteon morphotype scores using our scoring scheme (e.g., values lower than "5" in Fig. 1). At right is an image from the medial "compression" cortex that shows generally brighter osteons, which are quantified as higher osteon morphotype scores using our scoring scheme (e.g., "5" in Fig. 1). The breadth of each image is 1.4 mm. These images were obtained under the same illumination from PMMA-embedded and unstained sections that were ultramilled to a uniform thickness of 100 ± 5 μm.

The alpha value for statistical significance in these correlations was $\leq$0.0045, which also represents a correction to reduce spurious correlations.

RESULTS

Descriptive statistics and paired comparisons of osteon densities and percent areas, CFO/WMGLs, and osteon MTSs

Supporting Information Figures S2, S4, S6, S8, and S10 show means and standard errors of the osteon MTS, CFO/WMGL, secondary osteon population density (N.On/T.Ar), and percent area of secondary bone ([On.B.Ar/T.Ar]•100) data from the four cortical regions of five representative bones: deer calcanei, equine and sheep radii, equine MC3s, and chimpanzee femora. With the exception of the data from the chimpanzee femora, these osteon-related and CFO/WMGL data have been reported previously (Skedros et al., 2009). The results of the PP calculations are reported here for the first time for all of the bones and are shown in Supporting Information Figures S1, S3, S5, S7, and S9. In Figure 3 are representative CPL images from the medial "compression" and lateral "tension" cortices of a chimpanzee femur showing strain-mode-related differences in osteon morphotypes.

TABLE 1. ANOVA P *values for regional differences in collagen fiber orientation (CFO/WMGL), osteon morphotype score (MTS), various percent prevalence calculations*

Species and bone		CFO/WMGL	Six point osteon MTS	O/T	OI/T	OW/T	OWI/T
Deer calcaneus	Ant vs. Post	<0.001	<0.001	0.85	0.13	0.01	<0.001
	Med vs. Lat	0.05	0.09	0.65	0.20	0.71	0.15
Equine radius	Ant vs. Post	<0.001	<0.001	0.05	0.24	<0.001	<0.001
	Med vs. Lat	0.51	<0.001	0.20	0.01	0.01	0.12
Sheep radius	Ant vs. Post	0.01	0.70[a]	0.14	0.07	0.09	0.97
	Med vs. Lat	0.96	1.00	0.40	0.90	0.85	0.72
Equine MC3	Ant vs. Post	0.15	0.30	0.01	0.20	0.57	0.83
	Med vs. Lat	0.01	0.02	0.39	0.60	0.29	0.04
Chimpazee femur	Ant vs. Post	0.34	0.42	0.69	0.47	0.90	0.50
	Med vs. Lat	<0.001	0.01	0.10	0.03	0.32	<0.001
		(O+OI)/T	(OW+OWI)/T	% Hoop (O+OI+ OW+OWI)/T	D/T	N/T	% Hoop + N (O+OI+ OW+OWI+N)/T
Deer calcaneus	Ant vs. Post	0.21	<0.001	<0.001	<0.001	<0.001	<0.001
	Med vs. Lat	0.35	0.15	0.10	0.11	NA	0.11
Equine radius	Ant vs. Post	0.04	<0.001	<0.001	<0.001	<0.001	<0.001
	Med vs. Lat	0.74	0.01	<0.001	<0.001	NA	<0.001
Sheep radius	Ant vs. Post	0.01	0.26	0.40	0.30	0.18	0.30
	Med vs. Lat	0.53	0.88	0.59	0.75	0.24	0.75
Equine MC3	Ant vs. Post	0.01	0.70	0.01	0.01	0.47	0.01
	Med vs. Lat	0.31	0.12	0.90	0.28	0.71	0.86
Chimpanzee femur	Ant vs. Post	0.41	0.56	0.31	0.33	0.86	0.33
	Med vs. Lat	0.01	0.01	<0.001	<0.001	0.30	<0.001

Grayed cells = not statistically significant ($P > 0.0083$); MTS, morphotype score; Ant, anterior; Post, posterior; Med, medial; Lat, lateral; T, total osteons.
NA = not applicable because of insufficient number of osteons to perform these statistics.
See legend of Figure 1 or text for all other abbreviations.
[a] In our previous study we errantly reported this *P* Value as 0.11.

The results of regional comparisons showed that secondary osteon population densities (N.On/T.Ar) are greater in the "compression" cortex than in the "tension" cortex of the habitually bent radii ($P < 0.0083$) and calcanei (trend, $P = 0.01$) but not between the medial "compression" and lateral "tension" cortices of chimpanzee femora. By contrast, the chimpanzee femora had significantly different On.B/T.Ar (percent area of secondary bone) between their "compression" and "tension" cortices (Supp. Info. Fig. S10). However, unlike the radii where On.B/T.Ar was significantly greater in their "compression" cortices, On.B/T.Ar was significantly greater in the "tension" lateral cortex of the chimpanzee femur. This suggests that the osteons in the lateral cortex have larger diameters than those in the compression cortex (this parameter was not specifically quantified) (see Fig. 3).

The results of regional comparisons of CFO/WMGL are more consistent than the N.On/T.Ar and On.B/T.Ar data: CFO is predominantly longitudinal (dark WMGLs) in the "tension" cortices and predominantly oblique-to-transverse (brighter WMGLs) in the "compression" cortices of the habitually bent bones, including chimpanzee femora ($P \leq 0.001$) (the sheep radius showed a statistical trend, $P = 0.01$) (Table 1 and Supp. Info. Figs. S1–S9).

Descriptive statistics and paired comparisons of osteon percent prevalence data

As expected, there are no clear patterns in the PP calculations in the anterior/posterior or medial/lateral comparisons in the highly torsionally loaded equine MC3 (Supp. Info. Fig. S7) and sheep tibiae (data not shown). By contrast, all of the calcanei and the equine radii (Supp. Info. Figs. S1 and S3) show statistically significant and large differences (≥200%) between the anterior and posterior cortices (i.e., the "tension" and "compression" regions) in 70–80% of the 10 PP calculations. There are also statistically significant differences, but of relatively lower magnitude (29–108%), in only 50% of the 10 PP calculations between the medial "compression" and lateral "tension" cortices of the chimpanzee femora. These results show that the PP calculations do not reliably corroborate the significant strain-mode-related (tension vs. compression) differences shown in the CFO/WMGL and osteon MTS data. The percent prevalence calculations also failed to detect the statistical trends ($P = 0.01$) shown by the anterior "tension" vs. posterior "compression" CFO/WMGL difference in the sheep radii (Supp. Info. Fig. S5) and medial "compression" vs. lateral "tension" CFO/WMGL difference in the equine MC3s (Supp. Info. Fig. S7). As discussed in our previous study (Skedros et al., 2009), this statistical trend in the equine MC3 might reflect habitual medial/lateral bending in a majority of the bones in our sample.

Correlations of CFO/WMGL with osteon MTSs and with osteon percent prevalence data

As shown in our previous study (Skedros et al., 2009), regional variations in osteon MTS and CFO/WMGL data are typically highly and positively correlated in each of the "tension/compression" bones except for the sheep radius (Table 2). Explanations for the relatively weak, but positive, correlation in the sheep radii are discussed in our previous study (Skedros et al., 2009). In the chimpanzee femora and equine MC3s, where 60–90% of the PP calculations correlated significantly with CFO/WMGL, the majority of these calculations showed negative relationships. These results show that the osteon MTS and PP calculations are not as reliable as CFO/

TABLE 2. Correlations (r) of collagen fiber orientation (CFO/WMGL) with osteon morphotype score (MTS) and percent prevalence calculations

Species and bone	Six point osteon MTS	O/T	OI/T	OW/T	OWI/T	(O+OI)/T
Deer calcaneus	0.76	0.14	−0.09	−0.34	−0.78	−0.02
Equine radius	0.76	0.14	0.05	−0.56	−0.69	0.12
Sheep radius	0.34	0.44	−0.29	0.19	−0.43	−0.01
Equine MC3	0.67	−0.48	−0.45	−0.42	−0.38	−0.56
Chimpanzee femur	0.82	−0.24	−0.26	−0.35	−0.69	−0.33

	(OW+OWI)/T	% Hoop (O+OI+OW+OWI)/T	D/T	N/T	% Hoop + N (O+OI+OW+OWI+N)/T
Deer calcaneus	−0.77	−0.66	0.68	−0.49	−0.68
Equine radius	−0.76	−0.61	0.63	−0.41	−0.63
Sheep radius	−0.20	−0.18	0.21	−0.21	−0.21
Equine MC3	−0.47	−0.61	0.70	−0.29	−0.63
Chimpanzee femur	−0.73	−0.79	0.80	−0.21	−0.80

Grayed cells = not statistically significant ($P > 0.0045$); MTS, morphotype score; T, total osteons.
See legend of Figure 1 or text for all other abbreviations.

WMGL analyses for detecting strain-mode distributions associated with habitual bending.

DISCUSSION

The results of this study show that compared with various measures of the prevalence of the six osteon morphotypes, the osteon MTS and CFO/WMGL data more strongly correlated with strain-mode distributions produced by habitual bending. Because this relationship was shown clearly and most strongly in the proximal diaphyses of chimpanzee femora, these results expand our previous findings in artiodactyl, perissodactyl, and avian species showing that a history of habitual bending in diaphyseal regions can be inferred from the weighted scoring of secondary osteon morphotypes and/or predominant CFO in CPL images (Skedros and Hunt, 2004; Skedros et al., 2009). The consistency of these findings with respect to the primate and nonprimate bones suggests that the "interspecies differences" that tend to preclude comparative histological analyses in anthropological studies (e.g., comparing primate with artiodactyl bone) may be less restrictive in the context of these characteristics. Although there are examples where CFO/WMGL analyses have been shown to be useful for predicting strain-mode distributions of habitual bending when secondary osteons are few or absent (Mason et al., 1995; Skedros and Hunt, 2004), this method (typically) and the osteon morphotype scoring method (definitely) cannot be used in studies of bone adaptation during phases of growth or in some species or bones where osteon remodeling is infrequent or nonexistent (Skedros et al., 2003; McFarlin et al., 2008; Mulhern and Ubelaker, 2009). In other words, unlike CFO/WMGL analyses, osteon morphotype scoring is only reliable for detecting regional adaptation for bending when it is used in cases where the bone is sufficiently remodeled with secondary osteons (Riggs et al., 1993b; Skedros et al., 2007a).

Additional studies are needed to determine the extent to which a cortex must be remodeled (i.e., the fractional area of secondary bone, On.B/T.Ar) for the valid application of the osteon MTS and CFO/WMGL methods, and whether or not the "necessary" amount of remodeled cortex differs for their application. For example, the importance of this consideration is revealed by the highly birefringent (i.e., "bright") secondary osteons and nonosteonal bone (interstitial bone) in the medial "compression" cortices of the chimpanzee proximal femoral diaphyseal sections (see Fig. 3). In this case, the similar birefringence of the secondary osteons and the interstitial bone is included in CFO/WMGL data; hence, using this method, habitual compression could be detected even though the osteon density was lower than the opposing lateral "tension" cortex. By contrast, the birefringence of the interstitial bone in the medial cortex is not considered by the osteon MTS and other osteon-based quantification methods.

Osteon- and CFO-related measurements are finding increased use in studies that are aimed at inferring load history in bones or bone regions that are not amenable to in vivo strain measurement, including primate bones (Skedros and Kuo, 1999; Kalmey and Lovejoy, 2002; Goldman et al., 2003, 2009; Skedros et al., 2004, 2007b; McFarlin et al., 2008). As discussed in our recent study (Skedros et al., 2009), these correlative studies are couched in perspective of experimental biomechanical data showing that regional concentrations of specific osteon morphotypes and/or regional variations in predominant CFO are, independent of the mere presence of osteons, important for conferring mechanical "toughness" for nonuniform strain distributions (Riggs et al., 1993a,b; Hiller et al., 2003; Bigley et al., 2006; Skedros et al., 2006). Additional studies are needed to determine the influences that the more reliable characteristics—osteon MTSs and CFO/WMGL—have in affecting tissue mechanical properties of bone at a local level in additional contexts, including growth, aging, and metabolic stress. Investigations are also needed to determine if osteon MTSs and/or CFO/WMGL are potentially more revealing in studies where osteon density and related non-MTS or non-CFO/WMGL data have failed to show correlations with load history in the bones of humans and other primates (Drapeau and Streeter, 2006; Pfeiffer et al., 2006; McFarlin et al., 2008; Britz et al., 2009; Mulhern and Ubelaker, 2009).

Although in this study we usually found a localized increased prevalence of one osteon morphotype in a "tension" or "compression" region, we also observed heterogeneity in the distribution of some of the morpho-

types in addition to the presence of atypical morphotypes that were difficult to categorize in the scoring scheme. For example, we observed variably "hooped" osteons with "distributed" osteons in regions that are consistently loaded in compression, such as: (1) the medial cortex of the chimpanzee proximal femur and (2) the posterior cortex of the equine radius. In these cortical locations, the distributed (compression-adapted) osteon morphotype is expected. These observations show that one morphotype cannot be an exclusive diagnostic characteristic of a specific strain-mode environment (e.g., distributed osteons only for compression or strongly hooped osteons only for tension). We speculate that this is one reason why in many instances the PP calculations (typically based on subsets of the local osteon population) did not outperform the osteon MTS (based on a weighted score of all osteons of the local population). We also occasionally observed osteons that have features of both "weakly distributed" and "strongly hooped." Although these intermediate forms were rarely observed in the nonprimate species, their comparatively more frequent occurrence in the chimpanzee femora has prompted us to pursue additional studies where the osteon morphotype scoring scheme is expanded to include these intermediate and other distinctive morphotypes (e.g., osteons with variably "alternating" patterns of collagen birefringence).

Additional limitations in the use of PP calculations and osteon MTSs are also suggested by results in the sheep radii. In the sheep radii, the anterior "tension" and posterior "compression" cortices showed a statistical trend ($P = 0.01$) in the expected CFO/WMGL differences. The relatively small sample of seven bones appears to have provided insufficient statistical power to detect this comparison at $P < 0.0083$. None of the PP calculations showed this trend in the sheep radii (all P values > 0.2). Similarly, none of the PP calculations showed the trend ($P = 0.01$) that was revealed in the medial/lateral CFO/WMGL comparisons of the equine MC3s. As discussed previously (Skedros et al., 2009), this statistical trend might reflect a habitual strain distribution where the neutral axis rotates sufficiently to customarily load the medial cortex in prevalent/predominant compression and the lateral cortex in prevalent/predominant tension in the majority of our equine MC3s.

Osteon MTS and CFO/WMGL data in the chimpanzee proximal femoral diaphysis are consistent with habitual medial-lateral bending. Similarly, our previously reported CFO/WMGL data in adult human proximal femoral diaphyses suggest the presence of a medial-lateral (compression-tension) strain distribution in this region (Skedros et al., 1999). If these interpretations are correct, then this is an example of the utility of CFO/WMGL data for inferring habitual bending in primate bone regions where in vivo strain data are not available. An interesting finding in this perspective is that the results of this study did not reveal significant differences in the osteon population densities (N.On/T.Ar) between the medial and lateral cortices of the chimpanzee femora. This finding contrasts with the other habitually bent bones where N.On/T.Ar is typically higher in regions that are predominantly loaded in compression (Skedros et al., 2009). These results in the chimpanzee femur provide a poignant example of how N.On/T.Ar can be unreliable in detecting a habitual tension/compression strain-mode distribution in a diaphyseal region. In view of data from the nonprimate bones that we and others have studied previously (Skedros et al., 1994b; Takano et al., 1999; Skedros et al., 2009), we had considered it plausible that N.On/T.Ar might correlate positively with strain magnitude. During habitual bending of most bones, this means higher N.On/T.Ar in "compression" cortices because they receive the highest strain magnitudes. This occurs in most cases of bending because there is also sufficient eccentric axial compression to cause the neutral axis to shift toward the tension cortex, which reduces strains in this region while increasing strains in the opposing compression cortex (Lieberman et al., 2004). If variations in N.On/T.Ar are in fact correlated with strain magnitude, then the similar N.On/T.Ar in the medial and lateral chimpanzee femoral cortices suggests that the neutral axis passes in the vicinity of the anterior-posterior axis and not closer to the "tension" cortex as is typical in most habitually bent bones. In terms of possible mechanisms that produce the differences in osteon morphotypes and their population densities between regions of the same cross-section, perhaps a prevalent/predominant strain mode is more closely associated with the production of collagen/lamellar variations within osteons (osteoblastic functions) whereas strain-magnitude-related stimuli (e.g., microdamage) are stronger influences on the number and size of osteons (osteoclastic functions) (Takano et al., 1999; Skedros et al., 2004; van Oers et al., 2008; Britz et al., 2009). If this mechanistic distinction is correct, then regional strain-mode-related differences in collagen/lamellar construction within secondary osteons are produced by mechanisms that are independent of the mechanisms that govern formation frequencies of secondary osteons.

In summary, the osteon MTS more consistently showed positive and statistically significant correlations (or trends in the sheep radius) with regional predominant CFO in the habitually bent bones. By contrast, the PP calculations were less reliable in this context. Consequently, compared with the weighted scheme of the osteon MTS, regional variations in the PP of one or more specific osteon morphotypes: (1) are not stronger predictors of nonuniform strain-mode distributions produced by habitual bending and (2) are not stronger correlates of regionally predominant CFO. In this perspective, the osteon MTS score outperformed regional osteon PP calculations for interpreting cortical bone adaptation. However, the bones must be sufficiently remodeled with secondary osteons for the reliable application of this method. Experimental studies are needed to establish how much remodeling is "sufficient" in this context and to determine the relative sensitivities and specificities of the osteon MTS and CFO/WMGL for predicting functional adaptation in various contexts. Studies are also needed to determine if the general findings of this study can be corroborated in human limb bones.

ACKNOWLEDGMENTS

The authors thank Wm. Erick Anderson, Kyle Gubler, Jaxon Hoopes, Scott Sorenson, Adam Beckstrom, Kendra Keenan, Dr. Howard Winet, and Dr. Kenneth Hunt for their assistance in completing this study and/or their manuscript criticisms. They are indebted to Dr. Pat Campbell and Dr. Harlan Amstutz for the use of their laboratory facilities at the Joint Replacement Institute of Orthopaedic Hospital in Los Angeles, California.

LITERATURE CITED

Abbott S, Trinkaus E, Burr DB. 1996. Dynamic bone remodeling in later Pleistocene fossil hominids. Am J Phys Anthropol 99:585–601.

Ascenzi A, Bonucci E. 1968. The compressive properties of single osteons. Anat Rec 161:377–391.

Biewener AA, Thomason J, Goodship A, Lanyon LE. 1983. Bone stress in the horse forelimb during locomotion at different gaits: a comparison of two experimental methods. J Biomech 16:565–576.

Bigley RF, Griffin LV, Christensen L, Vandenbosch R. 2006. Osteonal interfacial strength and histomorphometry of equine cortical bone. J Biomech 39:1629–1640.

Bloebaum RD, Skedros JG, Vajda EG, Bachus KN, Constantz BR. 1997. Determining mineral content variations in bone using backscattered electron imaging. Bone 20:485–490.

Boyde A, Riggs CM. 1990. The quantitative study of the orientation of collagen in compact bone slices. Bone 11:35–39.

Britz HM, Thomas CD, Clement JG, Cooper DM. 2009. The relation of femoral osteon geometry to age, sex, height and weight. Bone 45:77–83.

Bromage TG, Goldman HM, McFarlin SC, Warshaw J, Boyde A, Riggs CM. 2003. Circularly polarized light standards for investigations of collagen fiber orientation in bone. Anat Rec B 274:157–168.

Drapeau MS, Streeter MA. 2006. Modeling and remodeling responses to normal loading in the human lower limb. Am J Phys Anthropol 129:403–409.

Emmanual J, Hornbeck C, Bloebaum RD. 1987. A polymethyl methacrylate method for large specimens of mineralized bone with implants. Stain Tech 62:401–410.

Goldman HM, Bromage TG, Thomas CD, Clement JG. 2003. Preferred collagen fiber orientation in the human mid-shaft femur. Anat Rec A 272:434–445.

Goldman HM, McFarlin SC, Cooper DM, Thomas CD, Clement JG. 2009. Ontogenetic patterning of cortical bone microstructure and geometry at the human mid-shaft femur. Anat Rec (Hoboken) 292:48–64.

Gross TS, McLeod KJ, Rubin CT. 1992. Characterizing bone strain distribution *in vivo* using three triple rosette strain gauges. J Biomech 25:1081–1087.

Hiller LP, Stover SM, Gibson VA, Gibeling JC, Prater CS, Hazelwood SJ, Yeh OC, Martin RB. 2003. Osteon pullout in the equine third metacarpal bone: effects of *ex vivo* fatigue. J Orthop Res 21:481–488.

Hinkle DE, Wiersma W, Jurs WG. 1979. Applied statistics for the behavioral sciences. Chicago, IL: Rand McNally College Pub. Co.

Hintze J. 2004. NCSS and PASS software. Kaysville, UT: Number Cruncher Statistical Systems.

Kalmey JK, Lovejoy CO. 2002. Collagen fiber orientation in the femoral necks of apes and humans: do their histological structures reflect differences in locomotor loading? Bone 31: 327–332.

Kuo T, Skedros JG, Bloebaum RD. 1998. Comparison of human, primate and canine femora: implications for biomaterials testing in total hip replacement. J Biomed Mater Res 40:475–489.

Kuo T, Skedros JG, Bloebaum RD. 2003. Measurement of the femoral anteversion by biplane radiography and ct imaging; comparison with an anatomic reference. Invest Radiol 38: 221–229.

Lanyon LE. 1974. Experimental support for the trajectorial theory of bone structure. J Bone Joint Surg B 56:160–166.

Lanyon LE, Baggott DG. 1976. Mechanical function as an influence on the structure and form of bone. J Bone Joint Surg B 58:436–443.

Lanyon LE, Bourn S. 1979. The influence of mechanical function on the development and remodeling of the tibia: an experimental study in sheep. J Bone Joint Surg A 61:263–273.

Lanyon LE, Magee PT, Baggott DG. 1979. The relationship of functional stress and strain to the processes of bone remodeling: an experimental study on the sheep radius. J Biomech 12:593–600.

Lieberman DE, Polk JD, Demes B. 2004. Predicting long bone loading from cross-sectional geometry. Am J Phys Anthropol 123:156–171.

Martin RB, Gibson VA, Stover SM, Gibeling JC, Griffin LV. 1996. Osteonal structure in the equine third metacarpus. Bone 19:165–171.

Mason MW, Skedros JG, Bloebaum RD. 1995. Evidence of strain-mode-related cortical adaptation in the diaphysis of the horse radius. Bone 17:229–237.

McFarlin SC, Terranova CJ, Zihlman AL, Enlow DH, Bromage TG. 2008. Regional variability in secondary remodeling within long bone cortices of catarrhine primates: the influence of bone growth history. J Anat 213:308–324.

Mulhern DM, Ubelaker DH. 2009. Bone microstructure in juvenile chimpanzees. Am J Phys Anthropol 140:368–375.

Neville AC. 1980. Optical methods in cuticle research. In Miller TA, editor. Cuticle techniques in arthropods. New York: Springer-Verlag. p 45–89.

Pfeiffer S, Crowder C, Harrington L, Brown M. 2006. Secondary osteons and haversian canal dimensions as behavioral indicators. Am J Phys Anthropol 131:460–468.

Riggs CM, Lanyon LE, Boyde A. 1993a. Functional associations between collagen fibre orientation and locomotor strain direction in cortical bone of the equine radius. Anat Embryol 187:231–238.

Riggs CM, Vaughan LE, Boyde A, Lanyon LE. 1993b. Mechanical implications of collagen fibre orientation in cortical bone of the equine radius. Anat Embryol 187:239–248.

Skedros JG, Baucom SL. 2007. Mathematical analysis of trabecular 'trajectories' in apparent trajectorial structures: the unfortunate historical emphasis on the human proximal femur. J Theor Biol 244:15–45.

Skedros JG, Bloebaum RD, Mason MW, Bramble DM. 1994a. Analysis of a tension/compression skeletal system: possible strain-specific differences in the hierarchical organization of bone. Anat Rec 239:396–404.

Skedros JG, Dayton MR, Sybrowsky CL, Bloebaum RD, Bachus K. 2006. The influence of collagen fiber orientation and other histocompositional characteristics on the mechanical properties of equine cortical bone. J Exp Biol 209:3025–3042.

Skedros JG, Demes B, Judex S. 2003. Limitations in the use of predominant collagen fiber orientation for inferring loading history in cortical bone. Am J Phys Anthropol Suppl 36:193.

Skedros JG, Hughes PE, Nelson K, Winet H. 1999. Collagen fiber orientation in the proximal femur: challenging Wolff's tension/compression interpretation. J Bone Miner Res 14: S441.

Skedros JG, Hunt KJ. 2004. Does the degree of laminarity mediate site-specific differences in collagen fiber orientation in primary bone? An evaluation in the turkey ulna diaphysis. J Anat 205:121–134.

Skedros JG, Hunt KJ, Bloebaum RD. 2004. Relationships of loading history and structural and material characteristics of bone: development of the mule deer calcaneus. J Morphol 259:281–307.

Skedros JG, Kuo TY. 1999. Ontogenetic changes in regional collagen fiber orientation suggest a role for variant strain stimuli in cortical bone construction. J Bone Miner Res 14:S441.

Skedros JG, Mason MW, Bloebaum RD. 1994b. Differences in osteonal micromorphology between tensile and compressive cortices of a bending skeletal system: indications of potential strain-specific differences in bone microstructure. Anat Rec 239:405–413.

Skedros JG, Mason MW, Nelson MC, Bloebaum RD. 1996. Evidence of structural and material adaptation to specific strain features in cortical bone. Anat Rec 246:47–63.

Skedros JG, Mendenhall SD, Kiser CJ, Winet H. 2009. Interpreting cortical bone adaptation and load history by quantifying osteon morphotypes in circularly polarized light images. Bone 44:392–403.

Skedros JG, Sorenson SM, Hunt KJ, Holyoak JD. 2007a. Ontogenetic structural and material variations in ovine calcanei: a model for interpreting bone adaptation. Anat Rec 290:284–300.

Skedros JG, Sorenson SM, Jenson NH. 2007b. Are distributions of secondary osteon variants useful for interpreting load history in mammalian bones? Cells Tissues Organs 185:285–307.

Skedros JG, Su SC, Bloebaum RD. 1997. Biomechanical implications of mineral content and microstructural variations in cortical bone of horse, elk, and sheep calcanei. Anat Rec 249:297–316.

Sokal RR, Rohlf FJ. 1995. Biometry. The principles and practice of statistics in biological research, 3rd ed. New York: W.H. Freeman and Co.

Su SC, Skedros JG, Bachus KN, Bloebaum RD. 1999. Loading conditions and cortical bone construction of an artiodactyl calcaneus. J Exp Biol 202 (Part 22):3239–3254.

Takano Y, Turner CH, Owan I, Martin RB, Lau ST, Forwood MR, Burr DB. 1999. Elastic anisotropy and collagen orientation of osteonal bone are dependent on the mechanical strain distribution. J Orthop Res 17:59–66.

Ural A, Vashishth D. 2006. Interactions between microstructural and geometrical adaptation in human cortical bone. J Orthop Res 24:1489–1498.

van Oers RF, Ruimerman R, van Rietbergen B, Hilbers PA, Huiskes R. 2008. Relating osteon diameter to strain. Bone 43:476–482.